Research Article | Vol. 29, No. 1 / 4 January 2021 / Optics Express 346
Optics EXPRESS

Mode-splitting in a microring resonator for self-referenced biosensing

M. DE GOEDE,[1] M. DIJKSTRA,[1] L. CHANG,[1] N. ACHARYYA,[2,6] G. KOZYREFF,[2] R. OBREGÓN,[3] E. MARTÍNEZ,[3,4,5] AND S. M. GARCÍA-BLANCO[1,*]

[1]*Optical Sciences Group, MESA+ Institute for Nanotechnology, University of Twente, P.O. Box 217, 7500 AE Enschede, The Netherlands*
[2]*Optique Nonlinéaire Théorique, Université libre de Bruxelles (U.L.B.), CP 231, Belgium*
[3]*Institutue for Bioengineering of Catalonia (IBEC), The Barcelona Institute of Science and Technology (BIST), Baldiri Reixac 10-12, 08028 Barcelona, Spain*
[4]*Department of Electronics and Biomedical Engineering, University of Barcelona (UB), Barcelona 08028, Spain*
[5]*Centro de Investigación Biomédica en Red (CIBER), Madrid 28029, Spain*
[6]*Max-Born-Institut für Nichtlineare Optik und Kurzzeitspektroskopie, D-12489 Berlin, Germany*
[*]*s.m.garciablanco@utwente.nl*

Abstract: Self-referenced biosensing based on mode-splitting on a microring resonator is experimentally demonstrated. A Bragg grating integrated on the surface of the ring provides coupling between the clockwise and counterclockwise travelling modes of the pristine ring resonator lifting their degeneracy. The amount of mode-splitting is directly related to the reflectivity of the grating and it is only affected by structurally modifying the grating. Environmental perturbations to the surroundings of the gratings, such as temperature and bulk refractive index variations, have a minor effect on the amount of mode-splitting. This principle allows the realization of a self-referenced sensing scheme based on the detection of variations of the mode-splitting induced by structural changes to the grating. In this work, a polymethyl methacrylate (PMMA) Bragg grating is integrated onto a ring resonator in Al_2O_3. It is shown both theoretically and experimentally that the amount of splitting of a resonance varies minimally under temperature or bulk refractive index perturbations. However, the structural change of attaching a layer of biomolecules inside the grating does affect its reflectivity and the amount of mode splitting present. This result represents the first proof-of-concept demonstration of an integrated mode-splitting biosensor insensitive to temperature and refractive index variations of the liquid matrix where the molecules to be detected are embedded. The reported results pave the road towards the realization of truly self-referenced biosensors.

1. Introduction

A strong demand exists for simple-to-use, label-free, portable, sensitive sensing systems that can be used for the detection of small particles, such as viruses or biomolecules, diluted in a fluid matrix for, among others, healthcare applications [1,2]. Optical ring resonators are excellent candidates to this goal [3–6]. Optical ring resonator sensors usually work by monitoring a shift of their resonance wavelength due to particle binding events, which elongate the optical path of the ring resonator. These devices have already been shown to provide label-free sensing of disease biomarkers from complex biological fluids down to clinically relevant levels [7–11]. Currently, most ring resonator sensors exhibit a limit of detection limited by environmental noise. The devices respond not only to the biomarker of interest, but also to all dielectric perturbations experienced by the ring resonators, including non-specific binding events, variations in temperature and in the bulk refractive index of the fluid matrix (e.g., urine,

#411931 https://doi.org/10.1364/OE.411931
Journal © 2021 Received 8 Oct 2020; accepted 1 Dec 2020; published 23 Dec 2020

Optics EXPRESS

plasma or blood). Different techniques to reduce the influence of these sources of noise have been proposed and implemented, including the use of reference rings [12,13], multi-mode differential sensing schemes [14] and frequency-locking for ultra-fast scanning, which allows to eliminate drifts and improve the signal-to-noise ratio [15].

Recently, a novel approach based on the splitting of the resonance modes of optical resonators has gained increasing attention. Optical resonators support two degenerate modes sharing the same resonance wavelength traveling in the counterpropagating clockwise (CW) and counterclockwise (CCW) directions. The binding of a scattering medium to the resonator provides mutual coupling between the CW and CCW modes, lifting their degeneracy resulting in a doublet splitting of the original resonant wavelength [16–18]. Using this transducing scheme, individual binding events of nanoparticles and even single viruses have been detected [19–21]. Since the variations of the mode splitting are due to the magnitude of the scattering, these sensors are to first-order insensitive to environmental variations such as temperature fluctuations or variations in bulk refractive index [22]. The mode-splitting induced by the introduction of reflective elements inside the resonator have been investigated [23–27]. Fiber Bragg gratings were introduced into fiber ring resonators to induce controlled mode-splitting [28,29]. This configuration was demonstrated as a strain sensor. Strain applied locally to the grating varies its reflectance and Bragg wavelength leading to changes in the magnitude of the mode splitting [30,31]. Coupling between the CW and CCW modes has also been demonstrated in microring resonators on silicon-on-insulator (SOI) by either self-coupling [32,33] and by means of a grating imposed onto the ring resonator [34–36]. Very recently, several theoretical schemes of self-referenced biosensing using grating-induced mode-splitting in microring resonators have been proposed [37,38].

In this paper, the first experimental demonstration of a self-referenced biosensor based on mode-splitting is presented. A Bragg reflector grating made of poly(methyl methacrylate) (PMMA) was fabricated on the surface of an aluminum oxide (Al_2O_3) ring resonator. The Al_2O_3 surface was functionalized to bind antibodies to selectively capture the S100A4 protein. This protein has been selected because it is related to human tumor development [39–41] and biosensors detecting this protein from a drop of urine down to clinically relevant levels have already been demonstrated [10,11]. The insensitivity of the proposed sensor to environmental perturbations such as temperature and bulk refractive index variations was demonstrated both theoretically as well as experimentally. Finally, a first proof-of-concept demonstration of the use of this sensor as a biosensor detecting the binding of both anti-S100A4 antibody as well as the S100A4 protein at different concentrations is successfully carried out. These results pave the road towards integrated optical biosensors that do not require strict temperature control, therefore enabling their use outside an optical laboratory setting.

2. Modelling of the self-referenced operation of a grating-integrated ring resonator

The considered structure is a bus waveguide coupled to a microring resonator with an integrated Bragg grating, as shown in Fig. 1(a). The reflectivity of the grating provides mutual coupling between the clockwise and counter clockwise propagating modes, resulting in mode-splitting, which is absent in the case of a pristine ring. The effect of the grating strength on the magnitude of the mode splitting is studied by varying the height of the teeth of the grating (Fig. 1(b)). The effect of environmental perturbations, such as temperature and bulk refractive index variations, on the mode-splitting are studied by varying the refractive indices, n, of the different materials according to their temperature coefficient of refractive index (dn/dT) and varying the refractive index of the surrounding medium, respectively (Fig. 1(b)). A semi-analytical model combining fully vectorial 2D eigenmode calculations (Lumerical MODE solutions) with the transfer matrix method, scattering matrix method and coupled mode theory [24,30] is utilized in this study.

Optics EXPRESS

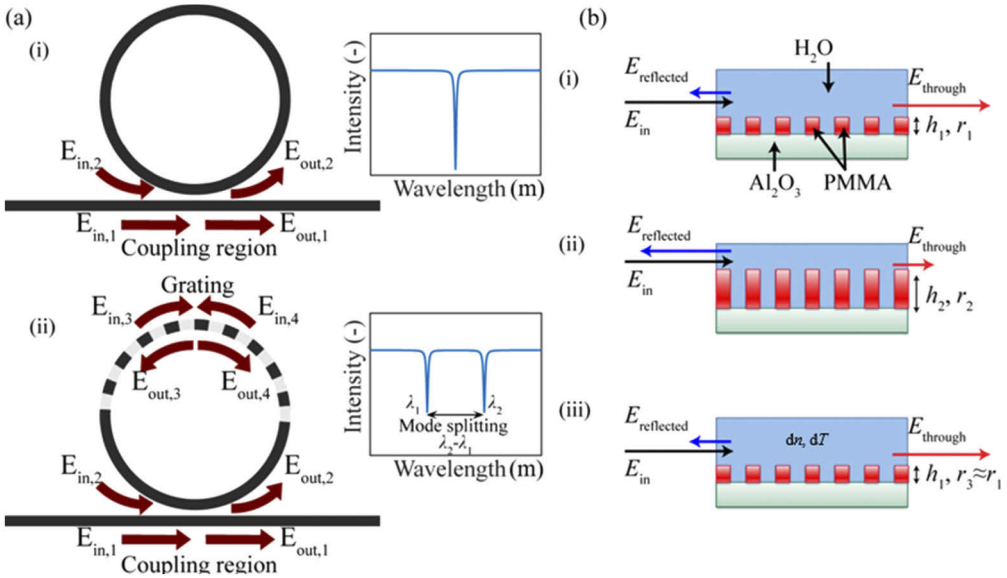

Fig. 1. (a) Microring resonator geometry with the travelling electric fields. (i) Pristine microring resonator. Inset shows one of its degenerate resonances. (ii) Microring resonator with grating. Inset shows one of its resonances exhibiting mode-splitting. (b) Effect of environmental variations applied to the grating. (i) Unperturbed grating with height h_1 and reflectivity r_1. (ii) Increasing the grating height to h_2 results in an increased reflectivity r_2. (iii) The reflectivity of the grating with height h_1 is almost invariant under temperature and bulk refractive index variations.

A schematic of the model is shown in Fig. 1(a). The field entering the bus waveguide via the input port excites the resonant modes of the microring via the directional coupler, which, assuming negligible loss, can be modelled as [24]:

$$\begin{pmatrix} E_{\text{out},1} \\ E_{\text{out},2} \end{pmatrix} = \begin{pmatrix} t & k \\ -k^* & t^* \end{pmatrix} \begin{pmatrix} E_{\text{in},1} \\ E_{\text{in},2} \end{pmatrix}, \tag{1}$$

with k and t the fractions of coupled and transmitted field amplitudes respectively. A lossless grating can be modelled by an unitary transfer matrix [24] as:

$$\begin{pmatrix} E_{\text{out},3} \\ E_{\text{out},4} \end{pmatrix} = \begin{pmatrix} \rho & \tau \\ \tau & \rho \end{pmatrix} \begin{pmatrix} E_{\text{in},3} \\ E_{\text{in},4} \end{pmatrix}, \tag{2}$$

where τ and ρ are the fractions of the amplitude of the electric field transmitted and reflected by the grating. These can be expressed as [30]:

$$\tau = \frac{\Theta}{\Theta\cosh(\Theta l_{\text{b}}) + j\Delta\beta\sinh(\Theta l_{\text{b}})}, \tag{3}$$

$$\rho = \frac{jK\sinh(\Theta l_{\text{b}})}{\Theta\cosh(\Theta l_{\text{b}}) + j\Delta\beta\sinh(\Theta l_{\text{b}})}, \tag{4}$$

where l_b is the length of the grating and Θ, $\Delta\beta$ and K are given by [30,42]:

$$\Theta = \sqrt{K^2 - \Delta\beta^2};\ \Delta\beta = \beta - \frac{\pi}{\Lambda};\ K = \frac{\Gamma(n_h^2 - n_l^2)\sin(\pi D)}{\lambda n_{\text{eff}}}, \tag{5}$$

Optics EXPRESS

where β is the propagation constant of the optical mode travelling inside the ring resonator, n_{eff} is its wavelength dependent effective refractive index, λ is the wavelength, Λ is the period of the grating, D is the filling fraction of a single grating period, Γ is the modal overlap of the optical mode with the grating region, and n_h and n_l are the alternating refractive indices of the materials inside the grating [42]. The length of the grating, l_b, is chosen to maximize the coverage of the microring while preventing overlap with both the directional coupler and the bus waveguide. The spectral transmission function of the microring resonator decorated with a Bragg grating can be derived as [24]:

$$T = \left| \frac{t - a\tau(1+t^2)e^{j\theta} - a^2 t e^{2j\theta}\det(S)}{1 - 2at\tau e^{j\theta} - a^2 t^2 e^{2j\theta}\det(S)} \right|^2, \tag{6}$$

where a and θ are respectively the attenuation of the electric field and the accumulated phase by the mode of the resonator after completing a single round trip and S is the scattering matrix of the grating. Whenever the reflected amplitude of the optical mode is sufficiently large, the resonance mode splits into two non-degenerate peaks at separate wavelengths λ_1 and λ_2. The mode-splitting $\Delta\lambda = \lambda_2 - \lambda_1$ can be derived from Eq. (7) and it is directly linked to the reflectivity, ρ, of the grating [24]:

$$\Delta\lambda = \frac{\lambda^2}{\pi n_{\text{eff}} L} \arctan\left(\sqrt{\frac{|\rho|^2}{1 - |\rho|^2}} \right) \tag{7}$$

where L is the perimeter of the microring resonator.

The effect of environmental and structural variations to the grating on the induced mode-splitting can be modelled. Both, changes in temperature as well as variations of bulk refractive index (i.e., refractive index of the liquid cladding over the sensor) vary the refractive indices of the different materials involved, and therefore, the effective refractive index of the guided mode inside the resonator and the mode overlap of the mode with the grating region (Γ). Using the perturbed values, the non-degenerated resonance wavelengths can be derived from the device transfer function, T. From Eq. (7), it can be clearly seen that changes in mode-splitting are due to variations of the reflectivity of the grating, which is mostly governed by Γ, which varies upon a change of the dielectric environment. The analysis is performed at a central wavelength of 1630 nm and it includes material and waveguide dispersion. At this wavelength, the refractive indices of the bottom SiO_2 cladding, Al_2O_3 waveguide and deionized H_2O top cladding are 1.443 [43], 1.668 (measured with Metricon 2010/M prism coupling setup) and 1.317 [44] respectively. The refractive index of PMMA at 1630 nm is 1.481 [45]. Temperature variations are included in the model by changing the refractive indices of the different materials using the thermo-optic coefficients dn/dT. For the materials utilized in the devices reported in this work, the temperature coefficients of refractive index are 1×10^{-5} K^{-1} [46], 1.9×10^{-5} K^{-1} [47], -4×10^{-5} K^{-1} [48] and -1.3×10^{-4} K^{-1} [49] for thermal SiO_2, Al_2O_3, H_2O and PMMA respectively. The temperature is varied in steps of 2.5 K. The bulk refractive index of the water top cladding is varied in steps of 0.001 RIU. The waveguide utilized in the modelling has a width of 2.2 µm and a thickness of 750 nm. A PMMA grating as the one depicted in Fig. 1(b) is considered, with a period of 535 nm, a fill factor of 0.5 and a coverage of 4/5 of the ring perimeter. The teeth of the grating have a height of 25 nm.

The response of the grating-decorated microring resonator was simulated and the results are shown in Fig. 2. The magnitude of the mode-splitting of the grating-integrated ring resonator only varies significantly when the reflectivity of the grating varies, as it is the case when the height of the teeth of the grating are varied (Fig. 2(a) and (b)). Mode-splitting only occurs from the onset of a specific grating height, for which the coupling rate exceeds the loss rates [50]. On the contrary, Figs. 2(c) and (d) show that the mode-splitting remains almost constant for bulk refractive index and temperature variations, with a sensitivity to refractive index variations of the bulk and temperature of 0.26 nm/RIU and −0.03 pm/K. Such small sensitivity to environmental

Optics EXPRESS

and temperature changes is due to the very low variation of the reflectivity of the grating with such perturbations, which hardly affect the mode overlap of the evanescent field with the grating. These results demonstrate theoretically that a grating-integrated ring resonator can be utilized as a self-referenced sensor provided that the sensing mechanism involves altering the structure of the grating. To maximize the sensitivity of the sensor to the binding of biomolecules to its surface, a grating with as high reflectivity as possible should be designed. This can be achieved by maximizing the coverage of the ring by the grating, using 50% filling ratio and optimizing the overlap of the optical mode with the grating region. Furthermore, the reflectivity of the grating should be minimized after binding of the saturation concentration of molecules (i.e., largest difference in reflectivity before and after binding).

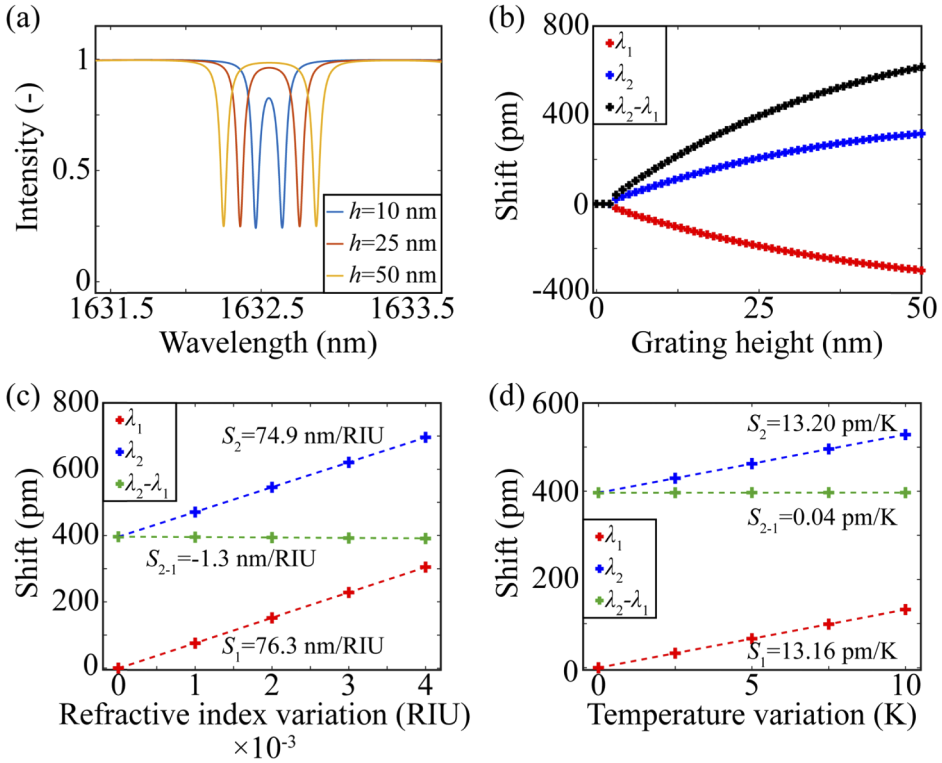

Fig. 2. (a) Transmission spectra of a grating-decorated microring resonator for varying heights of the PMMA grating on the surface of the resonator. (b) Wavelength shift with respect to the non-degenerate resonance wavelength of the microring of both non-degenerate modes for varying heights (h) of the PMMA grating. The mode splitting magnitude, λ_2-λ_1 is also shown. (c) Wavelength shift of both non-degenerate modes as well as their difference (i.e., mode-splitting) as a function of changes in the refractive index of the aqueous top cladding. (d) Wavelength shift of both non-degenerate modes as well as their difference (i.e., mode-splitting) as a function of temperature changes applied to the device. In both (c) and (d), the mode-splitting remains almost completely insensitive to changes of refractive index of the environment or changes in the temperature of the device. Furthermore, the higher resonance wavelength of the two modes (λ_2) is shifted by the value of the mode-splitting. Device dimensions: for (a)—(d): Al_2O_3 waveguide width is 2.2 µm and thickness is 750 nm; grating parameters: period of 535 nm, a fill factor of 0.5 and a coverage of 4/5 of the perimeter of the ring. Unless specified differently, the height of the teeth of the grating is 25 nm.

Optics EXPRESS

3. Device fabrication

An Al_2O_3 dielectric layer was deposited on a thermally oxidized silicon substrate (oxide thickness of 8 µm) with reactive sputtering in an AJA ATC 1500 machine, following the process described in [10,51]. The substrate temperature was set to 450°C. An RF power of 200 W was applied to an Al target. Gas flows of 2.5 sccm of reactive oxygen inside the chamber and 30 sccm of argon applied to the Al target were employed to a total process chamber pressure of 3.7 mTorr. The bus and ring resonator waveguides were then patterned using contact lithography (Olin OIR 906-12 photoresist and EVG 620 exposure tool) and subsequently reactively ion etched with a plasma of BCl_3 and HBr at a ratio of 5:2 and a total power of 25 W (Oxford Plasmalab System 100) [52]. Device parameters were a ring radius of 150 µm, coupling gap of 0.8 µm and waveguide cross section of ~0.8×2.4 µm^2. Then, a PECVD SiO_2 cladding layer 3 µm thick was deposited (Oxford Plasmalab 80 Plus, deposition temperature of 300 °C) using a shadow mask such that the ring resonator remains exposed to the environment, while the input and output bus waveguides and end facets are buried. The wafer was then diced into chips of dimensions ~1.2×1.9 cm^2 (Micro Ace 3) and cleaned with HNO_3, followed by rinsing with deionized water.

A PMMA Bragg grating was then printed over the device using electron beam lithography. This method was chosen due to its simple fabrication process only requiring the patterning and development of the grating, without any subsequent deposition or processing steps. Furthermore, the PMMA layer can easily be removed and the process repeated no-destructively, contrary to other implementations relying on etching a grating along the sidewall of the waveguide [34,35]. Figure 3(a) illustrates the process flow. First, a PMMA layer (NANO™ 950PMMA A4) was spun at 3.5 krpm for 1 minute to achieve a thickness of 30-40 nm on top of the waveguide. Then, a

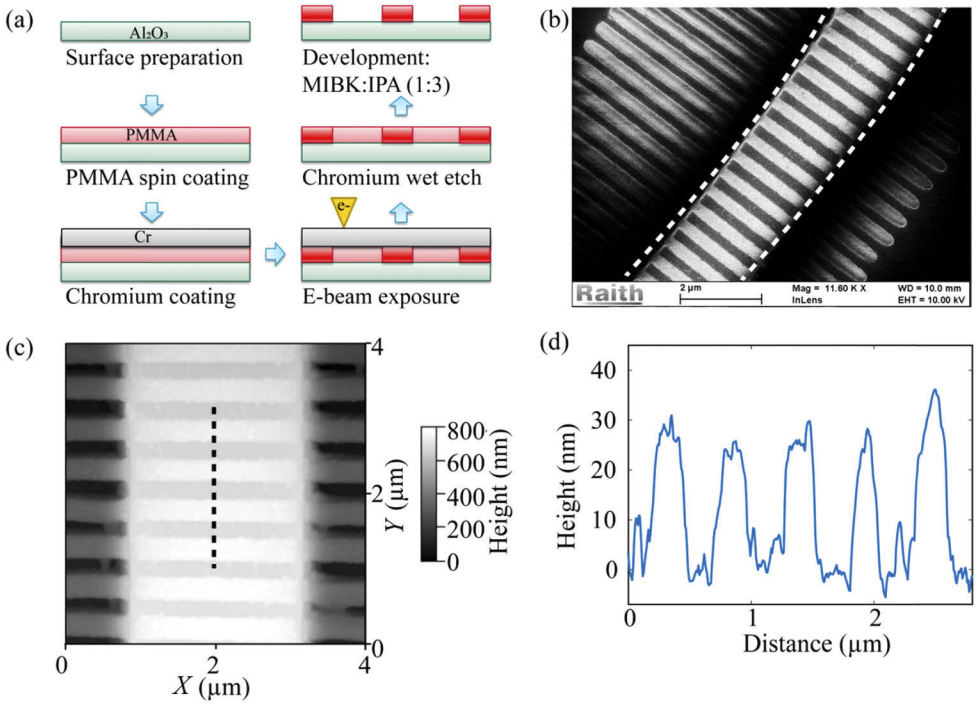

Fig. 3. Fabrication of the grating-integrated ring resonator. (a) Process flow. (b) SEM image of the developed PMMA grating. Dashed lines indicate the location of the waveguide sidewalls. (c) AFM scan of the PMMA grating on top of an Al_2O_3 waveguide. (d) Height profile of the PMMA grating along the dotted line in (c).

Optics EXPRESS

chromium coating ~5 nm thick was sputter coated using a homebuilt sputter coater at a power of 200 W and base pressure of 6.6×10^{-3} mBar. This layer prevents charging during the electron beam exposure, since both the substrate and the sample are non-conductive. Then, the grating pattern is exposed on top of the resist with a RAITH150 Two electron beam lithography tool. A dose of 180 μC/cm^2 was used, together with an acceleration voltage of 10 kV. The fabricated grating parameters were a period of 535 nm, a length of the grating of 4/5 of the circumference of the ring and a fill fraction of 0.35 (on the mask). After exposure and patterning, the Cr layer was removed by wet etch with a mixture of perchloric acid and ceric ammonium nitrate (TechniEtch Cr01) for 10 seconds, followed by a rinse in deionized water. The exposed PMMA is subsequently developed with a mixture of MIBK:IPA at a ratio 1:3 for 40 seconds, after which the device is rinsed with IPA for 20 seconds and blown dry with N_2. The resulting grating was imaged with SEM and AFM (Figs. 3(b) and (c)). The resulting PMMA grating has a fill factor of ~0.5. A height profile of the PMMA grating shows that the teeth are ~30 nm thick.

Finally, a PDMS microfluidic device consisting of a channel with dimensions of 600 μm width and 70 μm height was non-permanently bonded onto the chip and connected to a syringe pump to address the device with various liquids. The channel was then filled with deionized water to submerge the grating-integrated ring resonator.

4. Results and discussion

To optically characterize the device, its transmission spectrum was continuously recorded using an Agilent 81646 tunable laser (scan resolution of 1 pm and scan speed of 10 nm/s). The sample was held on a temperature controlled (~±0.0025°C) holder by vacuum. TE-polarized laser light was guided through single mode polarization maintaining fibers (PM1500-XP) and butt coupled to the sample using index-matching fluid. Figure 4 shows the transmission spectra of the same device covered in PMMA before and after grating fabrication. Before grating fabrication, the spectrum of the ring resonator contains multiple degenerate sharp resonances with quality factors Q up to 83×10^3. After fabrication of the grating, mode-splitting of the resonance modes is clearly observed. The magnitude of the mode-splitting varies along the bandwidth of the grating due to the variation of the reflectivity of the grating with wavelength. The measured maximum mode-splitting lies around a wavelength of 1627 nm and amounts to ~410 pm. The other resonance modes in the vicinity of 1627 nm experience also mode-splitting due to the relatively large bandwidth of the grating, which extends multiple free-spectral-ranges of the ring resonator. The mode-splitting reduces as the wavelength walks away from the Bragg wavelength. It can be observed that the resonances exhibit a lower Q due to extra scattering losses introduced during the fabrication of the grating.

The variation of the mode-splitting was measured upon applying environmental perturbations to the device. First, its temperature was varied while monitoring the positions of the degenerate resonance modes. Upon increasing the temperature of the stage holder, the whole transmission spectrum shifted to higher wavelengths, as shown in Fig. 5(a). However, since both wavelengths of the doublet shift to higher values, their mode-splitting remains almost constant as shown in Fig. 5(b). There are still some variations present in the magnitude of the mode-splitting, with a standard deviation around the mean of 0.5 pm, but these are more than a factor 100 lower than the wavelength shifts of the individual degenerate modes. This sensitivity is also two orders of magnitude lower than the temperature sensitivity of a passive microring resonator sensor in the same technology, as reported by us earlier [10]. This is illustrated by the almost identical slope sensitivities of both peaks of the doublet, as shown in Fig. 5(c). The same analysis was repeated by flowing various solutions of deionized water with NaCl concentrations dissolved in it to vary the refractive index of the liquid. Again, almost identical slope sensitivities are measured, as shown in Fig. 5(d). The sensitivity with respect to bulk refractive index changes is almost 3 orders of magnitude smaller than that of a passive microring resonator sensor without grating

Optics EXPRESS

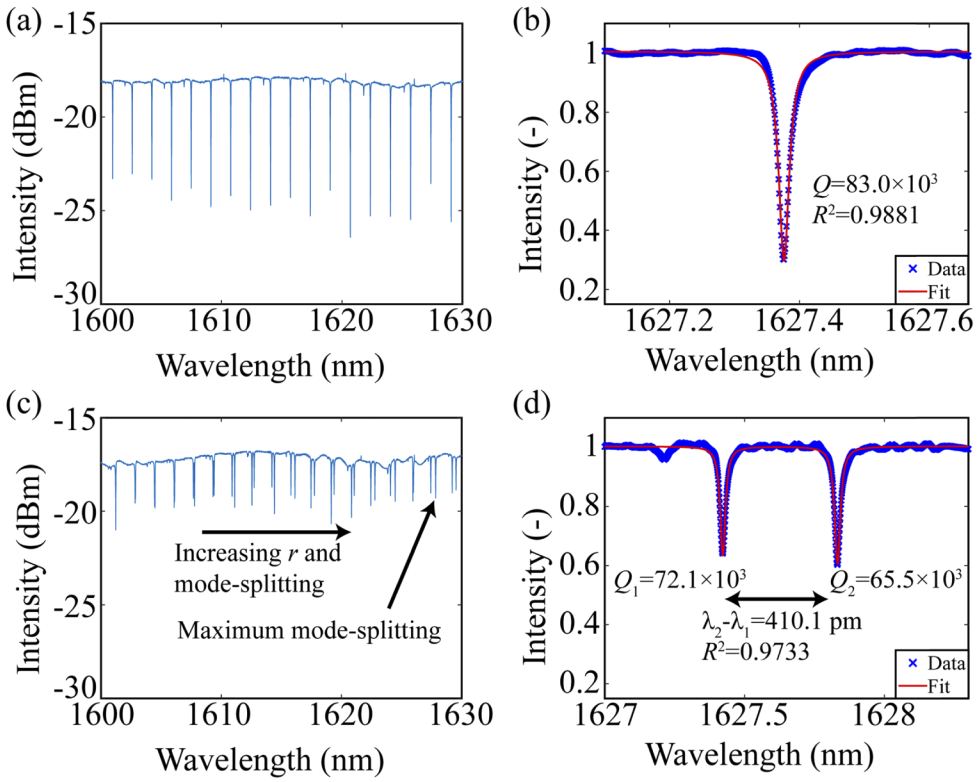

Fig. 4. (a) Transmission spectrum of a ring resonator covered in PMMA before grating patterning and development. (b) Zoom and fit of a degenerate mode from (a). (c) Transmission spectrum of the ring resonator after grating patterning and development. (d) Zoom and fit of maximum mode-splitting in (c).

[10]. These results, which match the results of the simulation shown in Fig. 2, indicate that the mode-splitting of the device does not vary upon applying environmental perturbations to the surroundings of the grating, demonstrating experimentally the self-referenced nature of the mode-splitting of a grating-integrated ring resonator.

The effect of the grating height on the mode-splitting was studied to show that the mode-splitting is only affected by variations of the grating structure through changes of its reflectivity, unlike the environmental variations that do not change the mode-splitting. Another grating was made with a different coupling coefficient (data not shown). The PMMA grating was stripped and its fabrication process was repeated, this time with a PMMA spin speed of 4 krpm in order to get a slightly thinner PMMA, and thus thinner grating. The rest of the exposure and development process was repeated with identical settings and the resulting grating structure had a thickness of ~25 nm, which should exhibit lower reflectivity due to the smaller overlap of the evanescent field with the grating. The maximum splitting now occurred at a slightly lower wavelength (1623 nm), since the thinner PMMA layer also lowers the effective index of the waveguide mode circulating in the ring resonator. The mode-splitting for this thinner grating was measured to be ~300 pm, showing that changing the structure of the grating results in a change of the mode-splitting.

The same device with grating thickness of ~25 nm was then used to perform a proof-of-concept demonstration of biosensing by modifying its mode-splitting through binding of biomolecules to alter the reflectivity of the grating. A three-step protocol to deposit the biomolecules inside the grating teeth was developed. The process is illustrated in Fig. 6(a). First, the sample and 200

Optics EXPRESS

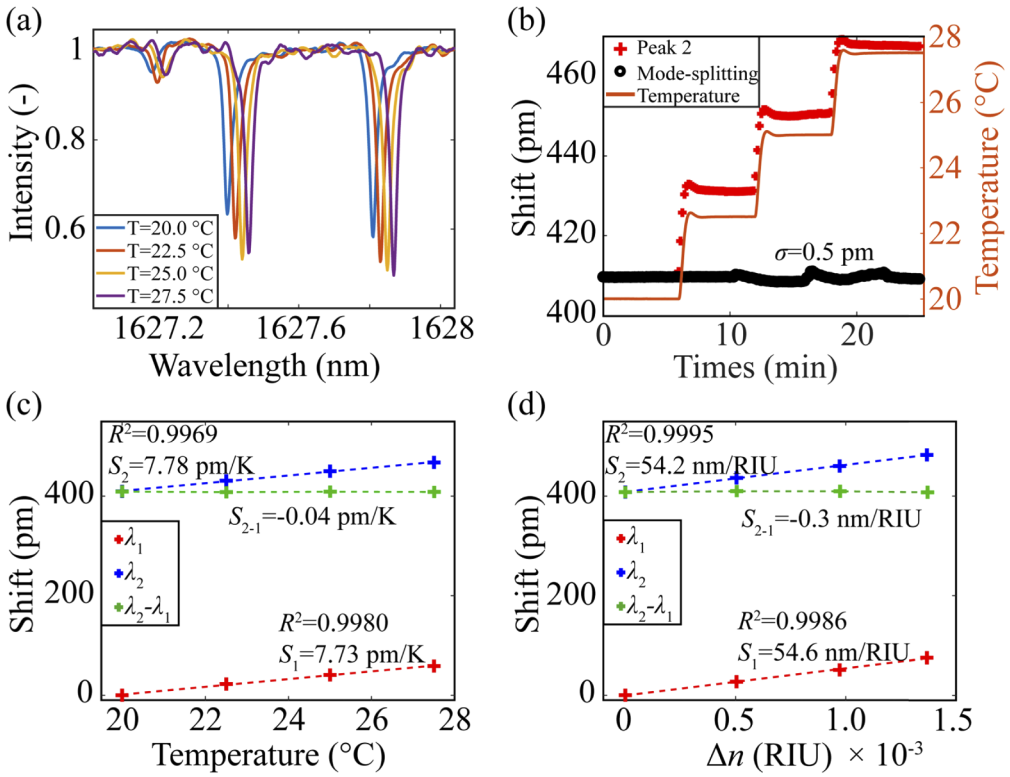

Fig. 5. Effect of dielectric perturbations to the surroundings of the grating. (a) Wavelength shifts of mode-split resonances upon applying temperature variations to the device. (b) Shift of one of the peaks in (a), together with the temperatures applied to the chip and the mode-splitting of the resonance. (c) Measured wavelength shifts of the two mode-split resonances for temperature variations applied to the device. (d) Measured wavelength shifts of the two mode-split resonances for bulk refractive index variations applied to the top cladding. The two mode-split resonances were referenced to the lower resonance wavelength of the modes (λ_1) at the initial conditions in both (c) and (d).

µl of (3-Glycidyloxypropyl)trimethoxysilane (GPTMS, Sigma Aldrich 440167) are placed in a desiccator for 4 hours to apply a silane functionalization through evaporation in gas phase. To validate the functionalization protocol, a fluorescence assay was carried out with an antibody labelled with fluorescein isothiocynate fluorescene dye (10 µg/ml), as shown in Fig. 6(b). The fluorescent signal originates mostly from the individual openings in the PMMA grating structure, indicating that the fluorescent antibodies bind mostly to the Al_2O_3 surface.

After applying the functionalization protocol, the device was exposed to a flow of 10 mM phosphate buffer saline (PBS) in order to establish a baseline. The amount of initial mode splitting was 297.6 pm. A solution of anti-S100A4 antibody at a concentration of 200 µg/ml in 10 mM PBS was prepared and flown over the device as shown in Fig. 6(c). All of the biomolecule solutions were flown at a rate of 30 µl/min for 20 minutes. Upon flowing the antibodies over the device, antibodies bonded to the grating result in a reduction of the mode-splitting. In this case, the mode-splitting is lowered from 297.6 to 288.4 pm. This is followed by a flow of the rhS100A4 proteins at concentrations of both 1 and 5 µM in 10 mM PBS. Mode-splitting variations of ~4 and ~6 pm respectively were measured. These changes are significantly larger than the noise

Optics EXPRESS

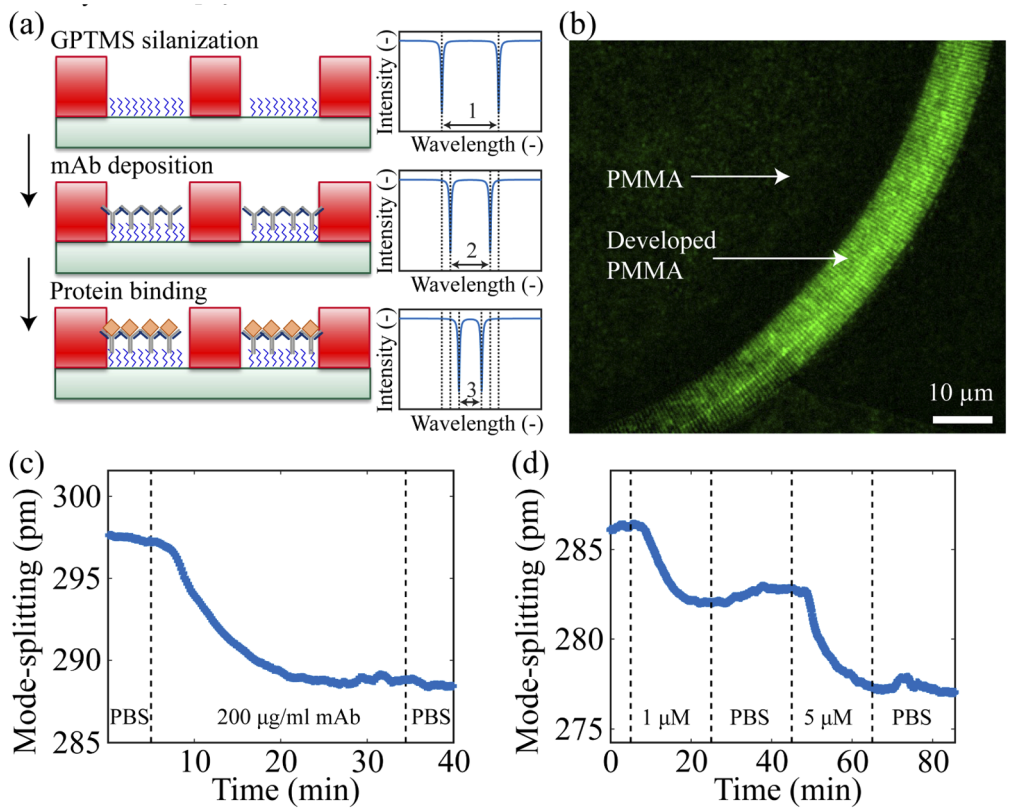

Fig. 6. (a) Surface functionalization protocol. GPTMS silanization is applied to the Al_2O_3 surface, followed by monoclonal antibody deposition and protein capture by the antibodies. (b) Microscope fluorescent image of the grating functionalized with GPTMS silane and immobilized with an antibody labelled with fluorescein isothiocyanate fluorescence dye (FITC, 495 nm/519 nm excitation/emission). Magnification 100x. (c) Change of mode-splitting upon antibodies binding to the grating. (d) Change of mode-splitting upon protein capture by the antibodies immobilized on the device.

present during the bulk sensing tests, indicating that the variation of the grating structure due to biomolecule attachment can be used for biomolecule detection.

The changes of the mode-splitting are rather small compared to the resonance wavelength shifts encountered in conventional ring resonator sensing. This is because the mode-splitting does not measure changes of the effective index of the mode travelling inside the ring, but changes of the grating reflectivity due to the presence of the biomolecules. Since these molecules are rather small with a low refractive index of ~1.5 [53], the effect on the grating is expected to be low. Furthermore, some of the antibodies and biomarkers can still bind to Al_2O_3 and PMMA through adsorption, lowering the relative change due to grating reflectivity modification. This type of sensor can perform better when larger target analytes are used, such as cancer biomarker extracellular vesicles [54], nanoparticles, bacteria, viruses or denser materials with a higher refractive index. Alternatively, a smaller microring radius could be used to increase the mode-splitting, and thus change upon biomolecule binding. A smaller waveguide cross-section could also increase the modal overlap with the grating and the biomolecules and yield a larger sensitivity upon binding on the grating reflectivity. One might also monitor the mode-splitting at a wavelength at the edge of the reflectivity spectrum instead of at the Bragg wavelength, where

Optics EXPRESS

the reflectivity profile is relatively flat. Then, a shift of both the resonance and Bragg wavelength results in the mode experiencing another reflectivity, which is accompanied by a change in mode-splitting [55]. Despite this scheme having an increased sensitivity, its self-referenced nature is cancelled. Finally, a promising solution was proposed in [38], where the ring is fully covered by a Bragg grating and the latter is functionalized only over a quarter of the perimeter. Then all the splitting can be concentrated on a single pair of degenerated modes, yielding sensitivities comparable to conventional schemes together and self-referenced operation.

5. Conclusions

This work describes a proof of principle of a self-referenced biosensor using a Bragg grating-integrated on a ring resonator. The Bragg grating lifts the degeneracy of the resonator modes resulting in mode-splitting, which depends on the reflectivity of the grating. The mode-splitting can be utilized as a sensor signal by varying the properties of the grating so that its reflectivity is modified. Since the grating reflectivity only varies very weakly for environmental perturbations such as temperature and bulk refractive index variations, the device can be used as a self-referenced sensor that has almost no response to dielectric perturbations of the bulk medium, whereas it provides a response to structural changes that do affect its reflectivity.

Here, a first experimental demonstration of a self-referenced integrated biosensor based on mode-splitting was successfully realized. The amount of splitting remained almost constant upon changing the temperature of the chip and the refractive index of the top cladding, cancelling their effect on the sensor signal. Biomolecules were immobilized inside the grating teeth, reducing the reflectivity of the grating and hence the amount of splitting of the resonance modes, allowing the device to be used for biosensing.

These results indicate the viability of using mode-split resonators not only for single-molecule and small-particle detection, but also for the self-referenced biosensing. Many future improvements can be performed to the device for enhanced sensitivity, and integration simplicity, paving the way for future sensing applications.

Funding

Horizon 2020 Framework Programme (634928).

Disclosures

The authors declare no conflicts of interest.

References

1. A. Mitra, B. Deutsch, F. Ignatovich, C. Dykes, and L. Novotny, "Nano-optofluidic detection of single viruses and nanoparticles," ACS Nano **4**(3), 1305–1312 (2010).
2. F. Patolsky, G. Zheng, O. Hayden, M. Lakadamyali, X. Zhuang, and C. M. Lieber, "Electrical detection of single viruses," Proc. Natl. Acad. Sci. **101**(39), 14017–14022 (2004).
3. W. Bogaerts, P. De Heyn, T. Van Vaerenbergh, K. De Vos, S. Kumar Selvaraja, T. Claes, P. Dumon, P. Bienstman, D. Van Thourhout, and R. Baets, "Silicon microring resonators," Laser Photonics Rev. **6**(1), 47–73 (2012).
4. J. Su, "Label-Free Biological and Chemical Sensing Using Whispering Gallery Mode Optical Resonators: Past, Present, and Future," Sensors **17**(3), 540 (2017).
5. X. Fan, I. M. White, S. I. Shopova, H. Zhu, J. D. Suter, and Y. Sun, "Sensitive optical biosensors for unlabeled targets: A review," Anal. Chim. Acta **620**(1-2), 8–26 (2008).
6. E. Kim, M. D. Baaske, and F. Vollmer, "Towards next-generation label-free biosensors: recent advances in whispering gallery mode sensors," Lab Chip **17**(7), 1190–1205 (2017).
7. A. L. Washburn, L. C. Gunn, and R. C. Bailey, "Label-free quantitation of a cancer biomarker in complex media using silicon photonic microring resonators," Anal. Chem. **81**(22), 9499–9506 (2009).
8. Y. Shin, A. P. Perera, and M. K. Park, "Label-free DNA sensor for detection of bladder cancer biomarkers in urine," Sens. Actuators, B **178**, 200–206 (2013).
9. J. T. Kindt and R. C. Bailey, "Biomolecular analysis with microring resonators: Applications in multiplexed diagnostics and interaction screening," Curr. Opin. Chem. Biol. **17**(5), 818–826 (2013).

Optics EXPRESS

10. M. de Goede, M. Dijkstra, R. Obregón, J. Ramón-Azcón, E. Martínez, L. Padilla, F. Mitjans, and S. García-Blanco, "Al_2O_3 microring resonators for the detection of a cancer biomarker in undiluted urine," Opt. Express **27**(13), 18508–18521 (2019).
11. M. de Goede, L. Chang, J. Mu, M. Dijkstra, R. Obrégon, E. Martínez, L. Padilla, F. Mitjans, and S. M. García-Blanco, "Al_2O_3:Yb^{3+} integrated microdisk laser label-free biosensor," Opt. Lett. **44**(24), 5937–5940 (2019).
12. G. Besselink, R. Heideman, E. Schreuder, L. Wevers, F. Falke, and H. Van den Vlekkert, "Performance of arrayed microring resonator sensors with the TriPleX platform," J. Biosens. Bioelectron. **7**(2), 1000209 (2016).
13. M. Iqbal, M. A. Gleeson, B. Spaugh, F. Tybor, W. G. Gunn, M. Hochberg, T. Baehr-Jones, R. C. Bailey, and L. Cary Gunn, "Label-Free biosensor arrays based on silicon scanning instrumentation," IEEE J. Sel. Top. Quantum Electron. **16**(3), 654–661 (2010).
14. X. Zhang, L. Liu, and L. Xu, "Ultralow sensing limit in optofluidic micro-bottle resonator biosensor by self-referenced differential-mode detection scheme," Appl. Phys. Lett. **104**(3), 033703 (2014).
15. J. Su, A. F. G. Goldberg, and B. M. Stoltz, "Label-free detection of single nanoparticles and biological molecules using microtoroid optical resonators," Light: Sci. Appl. **5**(1), e16001 (2016).
16. D. S. Weiss, V. Sandoghdar, J. Hare, V. Lefèvre-Seguin, J.-M. Raimond, and S. Haroche, "Splitting of high-Q Mie modes induced by light backscattering in silica microspheres," Opt. Lett. **20**(18), 1835 (1995).
17. A. Mazzei, S. Götzinger, D. S. Menezes, G. Zumofen, O. Benson, and V. Sandoghdar, "Controlled coupling of counterpropagating Whispering-Gallery modes by a single rayleigh scatterer: A classical problem in a quantum optical light," Phys. Rev. Lett. **99**(17), 173603 (2007).
18. B. E. Little, J. P. Laine, and S. T. Chu, "Surface-roughness-induced contradirectional coupling in ring and disk resonators," Opt. Lett. **22**(1), 4–6 (1997).
19. L. He, ŞK Özdemir, J. Zhu, W. Kim, and L. Yang, "Detecting single viruses and nanoparticles using whispering gallery microlasers," Nat. Nanotechnol. **6**(7), 428–432 (2011).
20. B.-B. Li, W. R. Clements, X.-C. Yu, K. Shi, Q. Gong, and Y.-F. Xiao, "Single nanoparticle detection using split-mode microcavity Raman lasers," Proc. Natl. Acad. Sci. **111**(41), 14657–14662 (2014).
21. J. Zhu, S. K. Ozdemir, Y. F. Xiao, L. Li, L. He, D. R. Chen, and L. Yang, "On-chip single nanoparticle detection and sizing by mode splitting in an ultrahigh-Q microresonator," Nat. Photonics **4**(1), 46–49 (2010).
22. L. He, S. K. Ozdemir, J. Zhu, and L. Yang, "Scatterer induced mode splitting in poly(dimethylsiloxane) coated microresonators," Appl. Phys. Lett. **96**(22), 221101 (2010).
23. A. Arbabi, Y. M. Kang, and L. L. Goddard, "Cylindrical coordinates coupled mode theory," IEEE J. Quantum Electron. **46**(12), 1769–1774 (2010).
24. J. Čtyroký, I. Richter, and M. Šiňor, "Dual resonance in a waveguide-coupled ring microresonator," Opt. Quantum Electron. **38**(9-11), 781–797 (2007).
25. Y. M. Kang, A. Arbabi, and L. L. Goddard, "A microring resonator with an integrated Bragg grating: A compact replacement for a sampled grating distributed Bragg reflector," Opt. Quantum Electron. **41**(9), 689–697 (2009).
26. Y. M. Kang, A. Arbabi, and L. L. Goddard, "Engineering the spectral reflectance of microring resonators with integrated reflective elements," Opt. Express **18**(16), 16813 (2010).
27. I. Teraoka, "A hybrid filter of Bragg grating and ring resonator," Opt. Commun. **339**, 108–114 (2015).
28. C. E. Campanella, L. Mastronardi, F. De Leonardis, P. Malara, G. Gagliardi, and V. M. N. Passaro, "Investigation of fiber Bragg grating based mode-splitting resonant sensors," Opt. Express **22**(21), 25371 (2014).
29. F. De Leonardis, C. E. Campanella, B. Troia, A. G. Perri, and V. M. N. Passaro, "Performance of SOI bragg grating ring resonator for nonlinear sensing applications," Sensors **14**(9), 16017–16034 (2014).
30. C. E. Campanella, A. Giorgini, S. Avino, P. Malara, R. Zullo, G. Gagliardi, and P. De Natale, "Localized strain sensing with fiber Bragg-grating ring cavities," Opt. Express **21**(24), 29435 (2013).
31. P. Malara, L. Mastronardi, C. E. Campanella, A. Giorgini, S. Avino, V. M. N. Passaro, and G. Gagliardi, "Split-Mode fiber Bragg grating sensor for high-Resolution static strain measurements," Opt. Lett. **39**(24), 6899–6902 (2014).
32. A. Pandey and S. K. Selvaraja, "Tunable coupling-induced resonance splitting in a self-coupled silicon ring cavity with robust spectral characteristics," Opt. Lett. **42**(14), 2854–2857 (2017).
33. A. H. Atabaki, B. Momeni, A. A. Eftekhar, E. S. Hosseini, S. Yegnanarayanan, and A. Adibi, "Tuning of resonance-spacing in a traveling-wave resonator device," Opt. Express **18**(9), 9447 (2010).
34. T. Wang, Z. Zhang, F. Liu, Y. Tong, J. Wang, Y. Tian, M. Qiu, and Y. Su, "Modeling of quasi-grating sidewall corrugation in SOI microring add-drop filters," Opt. Commun. **282**(17), 3464–3467 (2009).
35. Q. Huang, K. Ma, and S. He, "Experimental Demonstration of Single Mode- Splitting in Microring With Bragg Gratings," IEEE Photonics Technol. Lett. **27**(13), 1402–1405 (2015).
36. Z. Zhang, M. Dainese, L. Wosinski, and M. Qiu, "Resonance-splitting and enhanced notch depth in SOI ring resonators with mutual mode coupling," Opt. Express **16**(7), 4621 (2008).
37. K. Cicek and M. Cryan, "Spectral analysis of a four-port DBR micro-ring resonator for spectral sensing applications," J. Opt. **20**(8), 085803 (2018).
38. N. Acharyya, M. Maher, and G. Kozyreff, "Portable microresonator-based label-free detector: monotonous resonance splitting with particle adsorption," Opt. Express **27**(24), 34997–35011 (2019).
39. B. R. Davies, M. O'Donnell, G. C. Durkan, P. S. Rudland, R. Barraclough, D. E. Neal, and J. K. Mellon, "Expression of S100A4 protein is associated with metastasis and reduced survival in human bladder cancer," J. Pathol. **196**(3), 292–299 (2002).

Optics EXPRESS

40. Y. Sagara, Y. Miyata, T. Iwata, S. Kanda, T. Hayashi, H. Sakai, and H. Kanetake, "Clinical significant and prognostic value of S100A4 and matrix metalloproteinase-14 in patients with organ-confined bladder cancer," Exp. Ther. Med. **1**(1), 27–31 (2010).
41. F. Fei, J. Qu, M. Zhang, Y. Li, and S. Zhang, "S100A4 in cancer progression and metastasis: A systematic review," Oncotarget **8**(42), 73219–73239 (2017).
42. T. E. Murphy, "Design fabrication and measurement of integrated bragg grating optical filters," Massachusetts Institute of Technology (2001).
43. I. H. Malitson, "Interspecimen Comparison of the Refractive Index of Fused Silica," J. Opt. Soc. Am. **55**(10), 1205 (1965).
44. G. M. Hale and M. R. Querry, "Optical Constants of Water in the 200-nm to 200-µm Wavelength Region," Appl. Opt. **12**(3), 555 (1973).
45. G. Beadie, M. Brindza, R. A. Flynn, A. Rosenberg, and J. S. Shirk, "Refractive index measurements of poly(methyl methacrylate) (PMMA) from 0.4–1.6 µm," Appl. Opt. **54**(31), F139 (2015).
46. D. B. Leviton and B. J. Frey, "Temperature-dependent absolute refractive index measurements of synthetic fused silica," (July 2006), (2008).
47. C. C. Kores, N. Ismail, D. Geskus, M. Dijkstra, E. H. Bernhardi, and M. Pollnau, "Temperature dependence of the spectral characteristics of distributed-feedback resonators," Opt. Express **26**(4), 4892 (2018).
48. Y. H. Kim, S. J. Park, S.-W. Jeon, S. Ju, C.-S. Park, W.-T. Han, and B. H. Lee, "Thermo-optic coefficient measurement of liquids based on simultaneous temperature and refractive index sensing capability of a two-mode fiber interferometric probe," Opt. Express **20**(21), 23744 (2012).
49. Z. Zhang, P. Zhao, P. Lin, and F. Sun, "Thermo-optic coefficients of polymers for optical waveguide applications," Polymer **47**(14), 4893–4896 (2006).
50. Q. Li, T. Wang, Y. Su, M. Yan, and M. Qiu, "Coupled mode theory analysis of mode-splitting in coupled cavity system," Opt. Express **18**(8), 8367 (2010).
51. K. Worhoff, J. D. B. Bradley, F. Ay, D. Geskus, T. P. Blauwendraat, and M. Pollnau, "Reliable Low-Cost Fabrication of Low-Loss Al_2O_3:Er^{3+} Waveguides With 5.4-dB Optical Gain," IEEE J. Quantum Electron. **45**(5), 454–461 (2009).
52. J. D. B. Bradley, F. Ay, K. Wörhoff, and M. Pollnau, "Fabrication of low-loss channel waveguides in Al_2O_3 and Y_2O_3 layers by inductively coupled plasma reactive ion etching," Appl. Phys. B **89**(2-3), 311–318 (2007).
53. J. Vörös, "The density and refractive index of adsorbing protein layers," Biophys. J. **87**(1), 553–561 (2004).
54. W. Lee, A. Nanou, L. Rikkert, F. A. W. Coumans, C. Otto, L. W. M. M. Terstappen, and H. L. Offerhaus, "Label-Free Prostate Cancer Detection by Characterization of Extracellular Vesicles Using Raman Spectroscopy," Anal. Chem. **90**(19), 11290–11296 (2018).
55. P. Malara, C. E. Campanella, A. Giorgini, S. Avino, and G. Gagliardi, "Fiber Bragg grating laser sensor with direct radio-frequency readout," Opt. Lett. **41**(7), 1420 (2016).